S1 MA200 devices

Table S1. Manufacturer reported mass absorption efficiencies (MAE) of Black Carbon for MA200 devices.

Wavelength (nm)	Mass Absorption Efficiency ($m^2\ g^{-1}$)
375	24.069
470	19.070
528	17.070
625	14.091
880	10.120

S2 Analysis of the absorption Ångström exponent

Combustion sources such as wood burning and traffic emissions have distinct wavelength-dependent light absorption signatures, particularly in the ultraviolet and lower visible range. This characteristic fingerprint allows their contribution to be identified from the total measured absorption Zotter et al. (2017); Sandradewi et al. (2008); Massabò et al. (2015); Bernardoni et al. (2017). The absorption Ångström exponent (α) serves as a single parameter to quantify the source-specific dependence of light absorption coefficient on wavelength. In the absence of validation measurements, the α frequency distribution can guide the estimation of suitable α values for the source apportionment model. Figure S1 shows the probability density function of α for the hourly aggregated measurements during the two periods analysed in the main text, i.e. from 4 February to 7 March 2020 and from 26 December 2020 to 21 January 2021 at the traffic site, and from 4 February to 7 March 2020 and from 26 December 2020 to 7 January 2021 at the background site. Data reported with light blue colour are calculated as follow:

$$\alpha = -\frac{\log(b_{880}/b_{375})}{\log(880/375)}$$

Where b_{880} and b_{375} are the absorption coefficients at 880 nm and 375 nm respectively. While the data shown in grey are obtained by fitting the absorption coefficient as a function of the five wavelengths (375, 470, 528, 625 and 880 nm) with a filter of $r^2 > 0.99$ to the fit. In addition, a subplot for the traffic site has been incorporated under its facet, showing α values only for the morning rush hour (08:00 GMT time) on working days, i.e. when the traffic contribution is expected to be at its peak. For traffic, the source-specific α value is set to 1, which corresponds to the centre of the probability density function (PDF) distribution for the morning rush hour on working days at the traffic site. Conversely, the α value for biomass burning is set to 2, representing the upper tail of the stringent-filtered PDF distribution for both traffic and background sites, as suggested by Tobler et al. (2021).

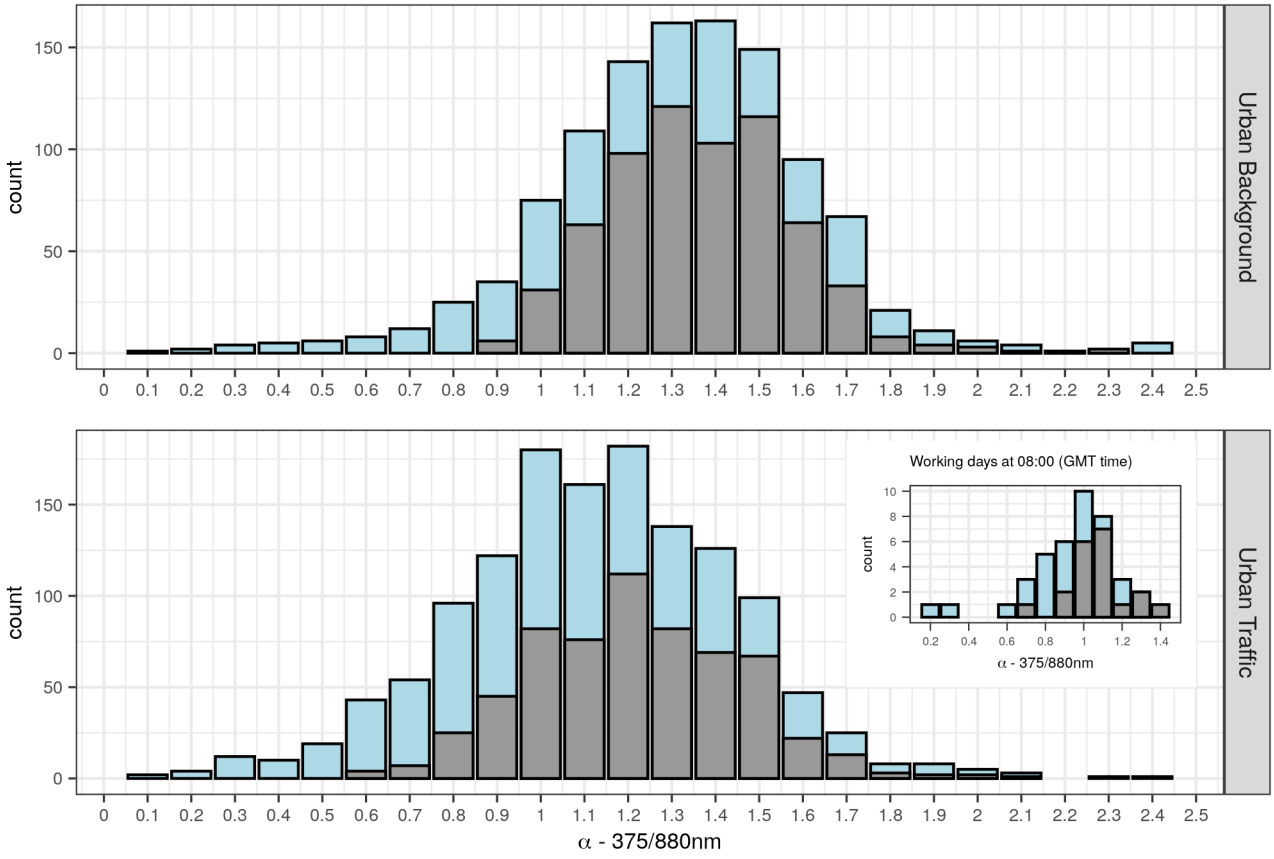

Figure S1. The absorption Ångström exponent (α) probability density function calculated from the ratio of the 375 nm and 880 nm wavelengths and from the fit off all wavelengths from 375 nm to 880 nm and filtered for fit $r^2 > 0.99$.

S3 BC speciation factors

Table S2. BC speciation factors from $PM_{2.5}$ emissions.

Emission Sector	Emission activity	Fuel	BC/$PM_{2.5}$ (%)
Energy production	all	liquid	56
Energy production	all	biomass and agricultural residues	6.4
Energy production	all	CNG	4
Domestic heating	open fireplaces	biomass	7
Domestic heating	conventional stoves burning	biomass	10
Domestic heating	high-efficiency stoves	biomass	16
Domestic heating	advanced/ecolabelled stoves and boilers	biomass	28
Domestic heating	pellet stoves and boilers	biomass	15
Domestic heating	all	CNG	5.4
Industry	all	solid fuel	6.4
Industry	all	CNG	4
Industry	all	liquid	56
Other mobile machinery	all	liquid	70
Waste management	incinerator	all	20

S4 Model evaluation

To evaluate the performance of the models in reproducing BC concentrations and wind speed, several statistical indicators were considered. These indicators were derived by considering M as the modelled values, O as the observations, n as the count of model-observation pairs,

$$\bar{M} = \frac{1}{n}\sum_{i=1}^{n} M_i$$

as the average modelled value, and

$$\bar{O} = \frac{1}{n}\sum_{i=1}^{n} O_i$$

as the average observed value. The following metrics were employed for evaluation:

$$MB = \frac{1}{n}\sum_{i=1}^{n}(M_i - O_i)$$

$$NMB = \frac{1}{n}\sum_{i=1}^{n}\frac{(M_i - O_i)}{O_i}$$

$$r = \frac{\sum_{i=1}^{n}(M_i - \bar{M})(O_i - \bar{O})}{\sqrt{\sum_{i=1}^{n}(M_i - \bar{M})^2 \sum_{i=1}^{n}(O_i - \bar{O})^2}}$$

$FAC2 =$ Fraction of data where $0.5 \leq \frac{M_i}{O_i} \leq 2$

$$NMSE = \frac{\overline{(O - M)^2}}{\bar{O} \cdot \bar{M}}$$

$$FB = \frac{\overline{O - M}}{0.5 \cdot (\bar{O} + \bar{M})}$$

$$NAD = \frac{\overline{|O - M|}}{(\bar{O} + \bar{M})}$$

$$RMSE = \sqrt{\frac{1}{n}\sum_{i=1}^{n}(M_i - O_i)^2}$$

S5 Meteorological analysis

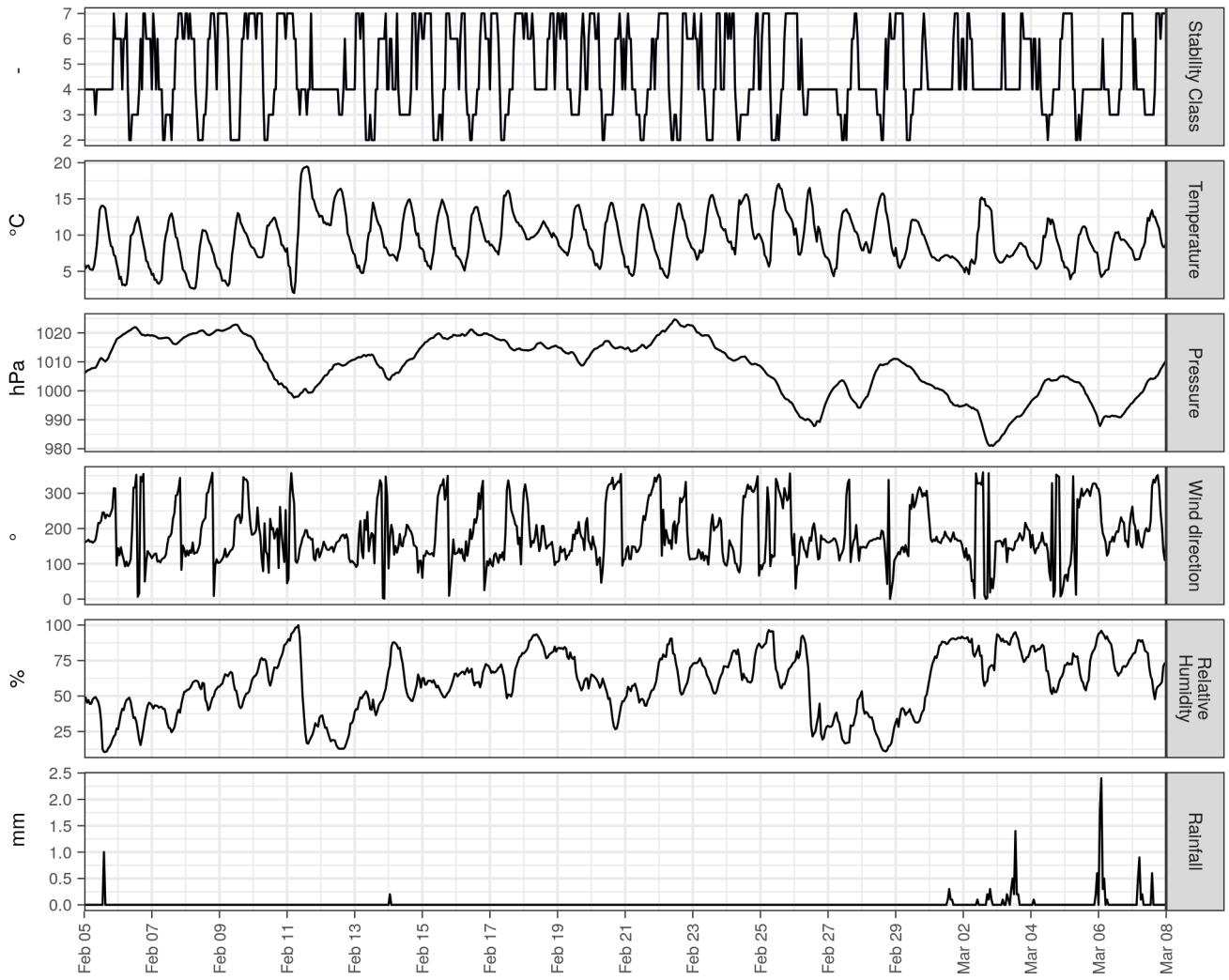

Figure S2. Hourly time series of measured (temperature, pressure, wind direction, relative humidity, rainfall) and estimated (stability class) meteorological parameters during the first period (4 February - 7 March 2020) at OSS station.

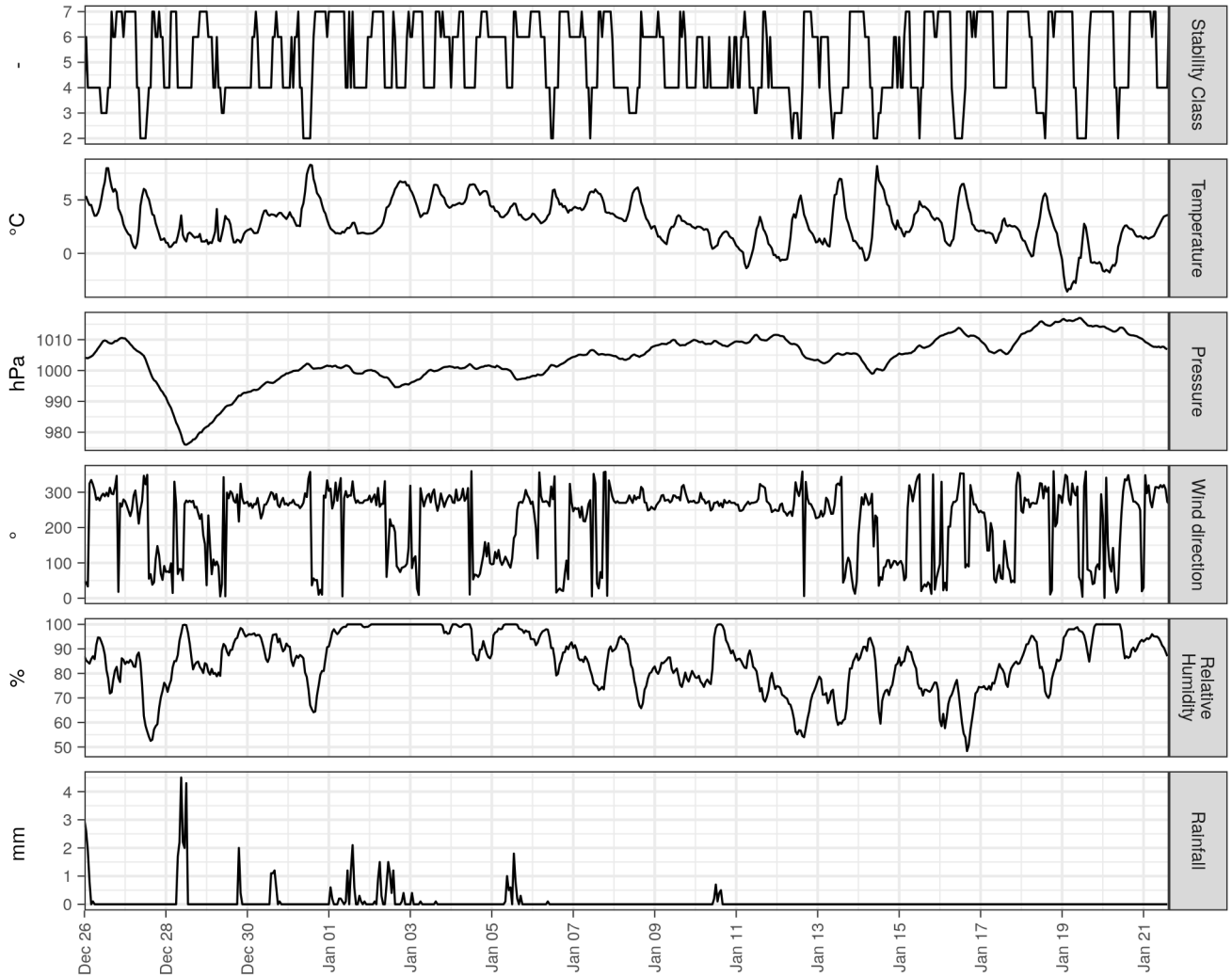

Figure S3. Hourly time series of measured (temperature, pressure, wind direction, relative humidity, rainfall) and estimated (stability class) meteorological parameters during the second period (26 December 2020 - 21 January 2021) at OSS station.

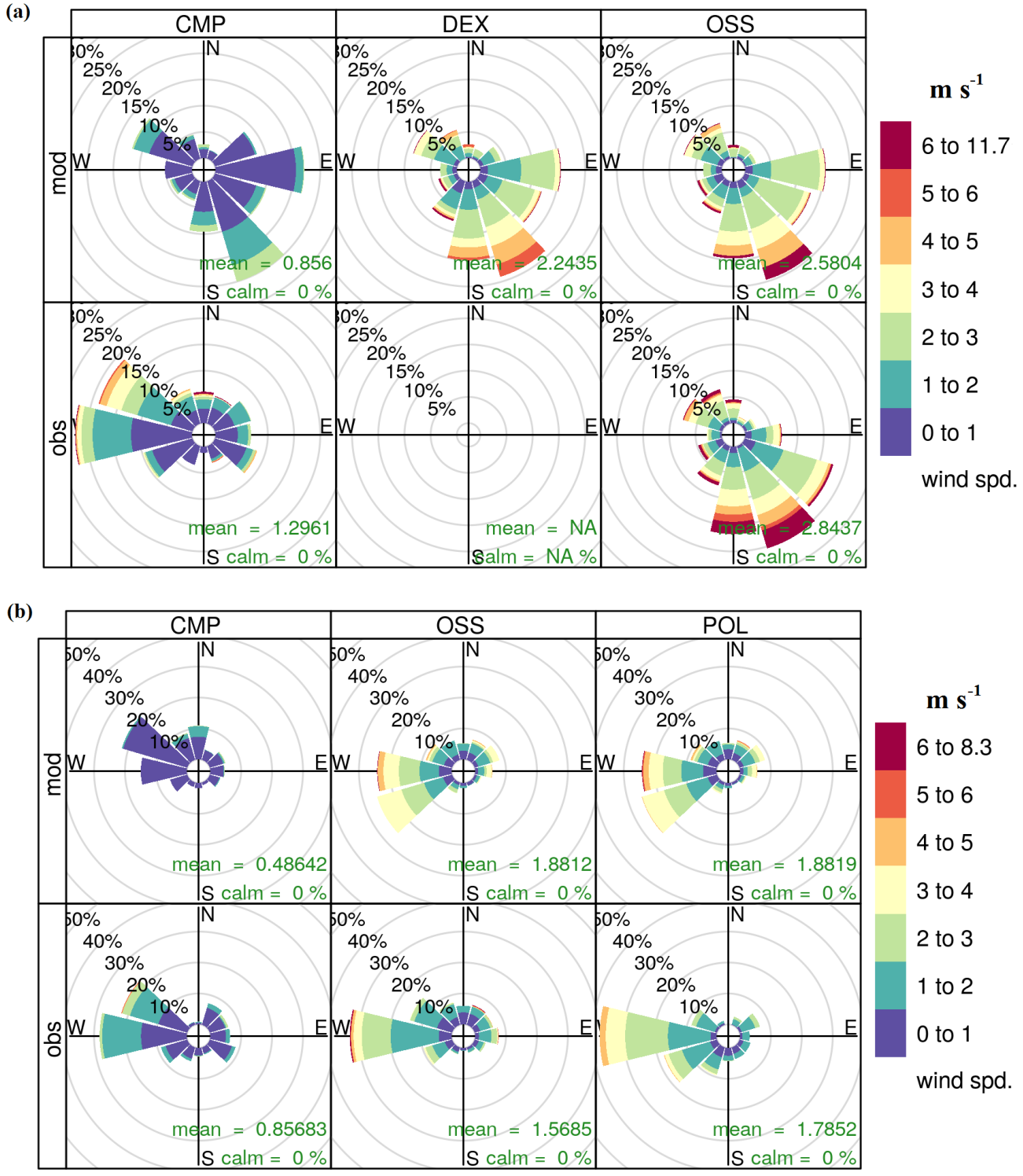

Figure S4. Comparison of modelled (mod) and observed (obs) wind roses at CMP, OSS, DEX and POL stations for the two simulation periods: (a) first period (4 February - 7 March 2020) and (b) second period (26 December 2020 - 21 January 2021). Wind direction data from DEX station during the first period were excluded from the analysis due to a significant data gap and observed biases in the sensor readings.

S6 Analysis of specific pollution episodes

During the second period of this study (between 26 December 2020 and 21 January 2021), favourable meteorological conditions for the accumulation of pollutants were observed in Modena and the surrounding area, such as predominantly calm episodes, exacerbated by high pressure systems and persistent temperature inversions in the first layers of the atmosphere. Looking more closely at certain days, namely 3, 13-14 and 18-19 January 2021, significant peaks in BC levels were observed. At the traffic site the peak concentrations on these days were 14.1 $\mu g\,m^{-3}$, 18.5 $\mu g\,m^{-3}$ and 16.3 $\mu g\,m^{-3}$. It is worth noting that the episode on 3 January was observed exclusively at the traffic site, while the total PM_{10} and $PM_{2.5}$ concentrations recorded at the same two locations of the MA200 observations were typical for the period, without notable peaks (Figure S4). Specifically, PM_{10} levels were 31 $\mu g\,m^{-3}$ and 25 $\mu g\,m^{-3}$ at the traffic and background stations respectively, while $PM_{2.5}$ was 14 $\mu g\,m^{-3}$ at the background station. Furthermore, the meteorological conditions on this particular day were not particularly conducive to the accumulation of pollutants. This can be seen from the vertical temperature profile derived from soundings at 00:00 and 12:00 GMT at SPC, Figure S5. A shallow inversion layer is present only in the first 40 m above the ground, then the temperature gradually decreases with height following a profile similar to dry adiabats at both 00:00 and 12:00 GMT. In addition, other meteorological parameters measured at OSS were not consistent with conditions favourable for a specific episode (see Fig. S2). A plausible explanation for this peak could be the presence of high-emitting vehicles passing close to the station along the busy road or vehicles idling in nearby car parks, the latter phenomenon also reported in a previous study focused on the same area (Ghermandi et al., 2019). To further support this hypothesis, it is worth highlighting that this particular episode had a remarkably short duration, lasting only a single hour (Figure 5 in the main text). After this short interval, BC concentrations returned to levels characteristic of the traffic site.

When analysing the other two periods, namely 13-14 and 18-19 January 2021, the dynamics were different. While direct BC data at the background site are not available for this period, the total PM_{10} and $PM_{2.5}$ concentrations (Figure S4) confirmed the presence of meteorological and emission conditions conducive to pollutant accumulation. Figure S2 shows a significant increase in atmospheric pressure at OSS, suggesting the possible establishment of a high pressure system in the area. This atmospheric scenario was accompanied by calm and stable meteorological conditions, with an average wind speed of less than 2.5 $m\,s^{-1}$, as shown in Figure 3 (panel b). Furthermore, these conditions contributed to the formation of temperature inversions not only during the night hours, but also during the day, as shown in Figures S6 and S7. Taken together, these conditions probably facilitated the accumulation of pollutants close to the ground, thereby limiting both their vertical and horizontal dispersion. Comparable meteorological conditions were also observed on 16 January 2021, in contrast to the previously analysed days, which fall on a Saturday and typically have reduced anthropogenic emissions from traffic and industrial activities compared to weekdays. Consequently, the BC and PM concentrations on this particular day were lower than those recorded on 13-14 and 18-19 January 2021.

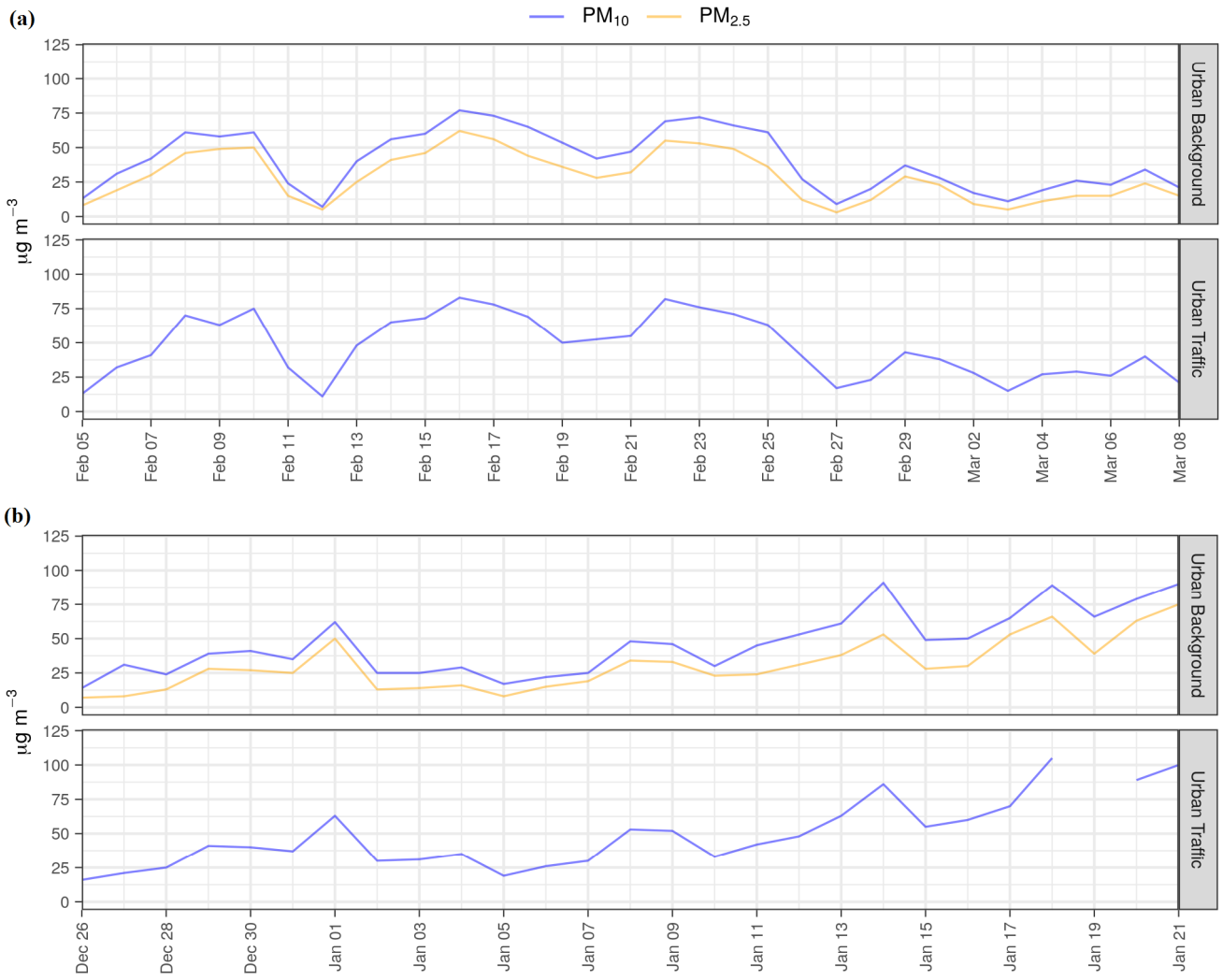

Figure S5. Daily time series of measured PM_{10} and $PM_{2.5}$ concentrations at urban traffic and background sites for the first period, panel (a), and the second period, panel (b).

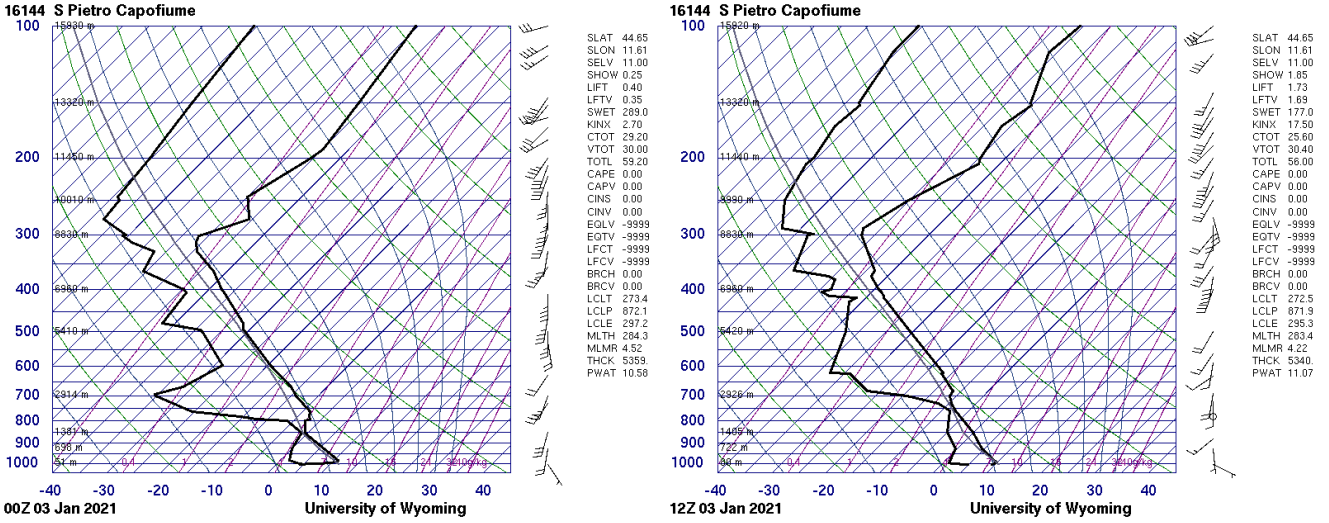

Figure S6. Skew-T Log-P plot from S. Pietro Capofiume station on 3 January 2021 at 00:00 GMT, on the left, and at 12:00 GMT on the right.

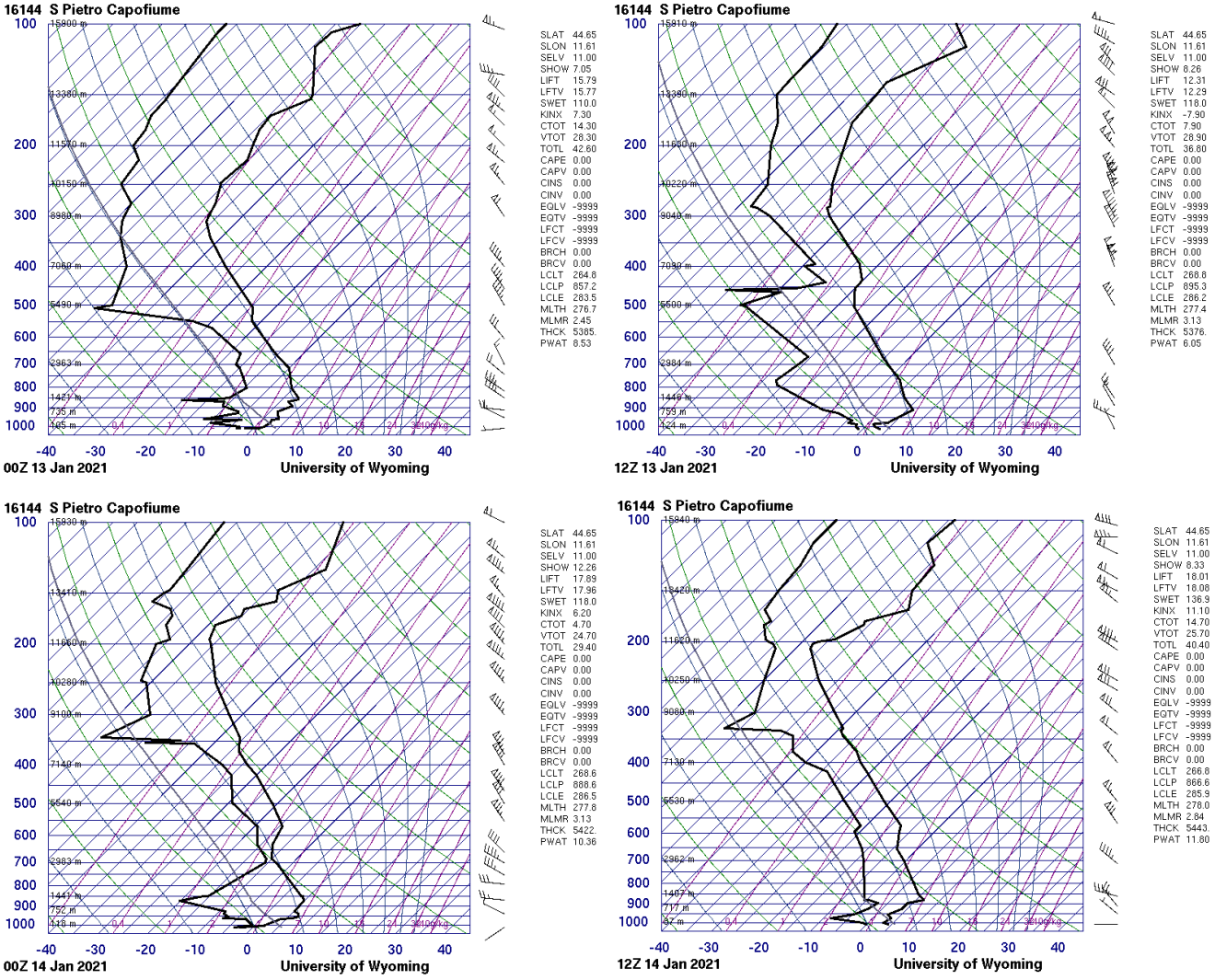

Figure S7. Skew-T Log-P plot from S. Pietro Capofiume station on 13 January 2021 on the first row and on 14 January 2021 on the second row, at 00:00 GMT on the left, and at 12:00 GMT on the right.

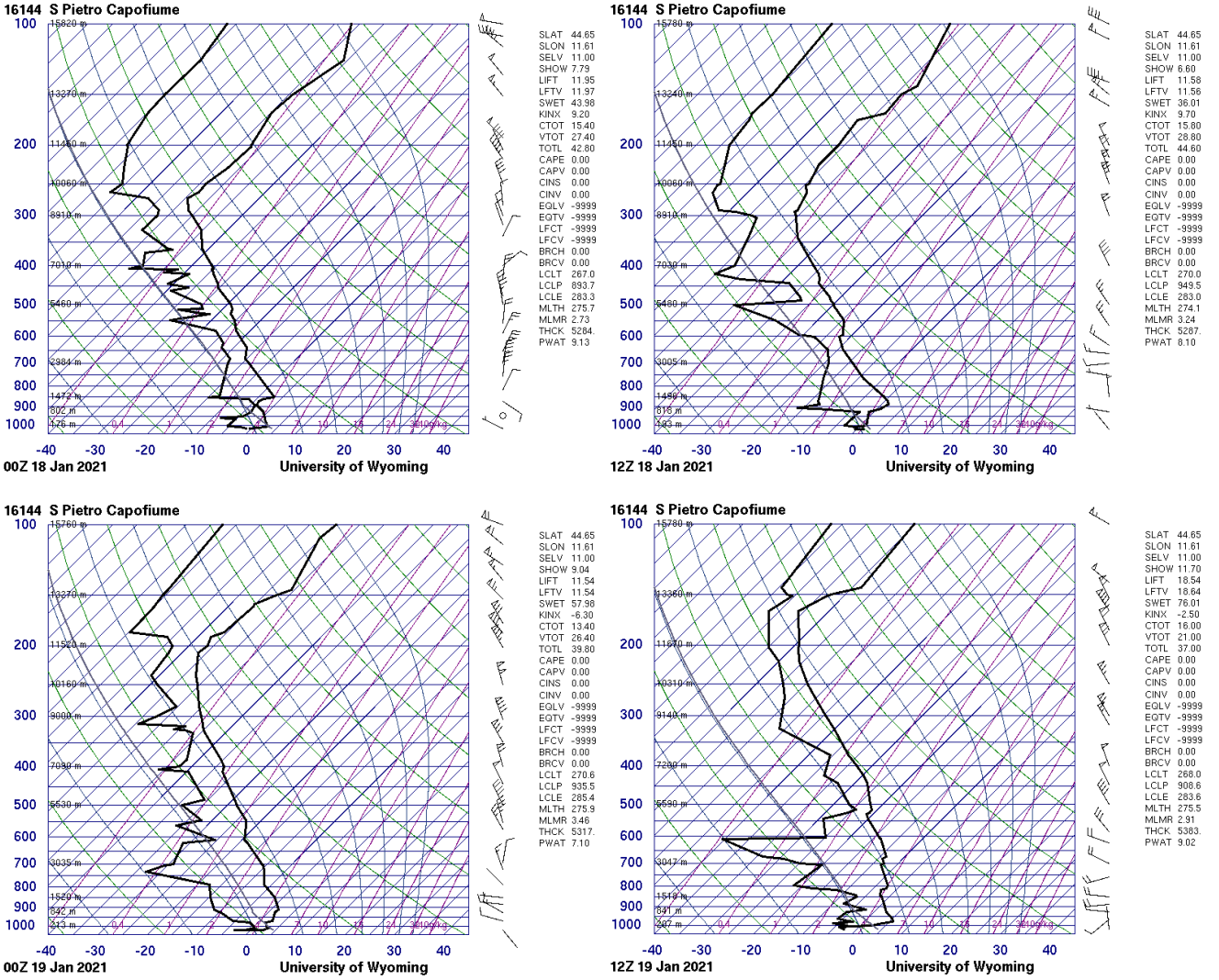

Figure S8. Skew-T Log-P plot from S. Pietro Capofiume station on 18 January 2021 on the first row and on 19 January 2021 on the second row, at 00:00 GMT on the left, and at 12:00 GMT on the right.

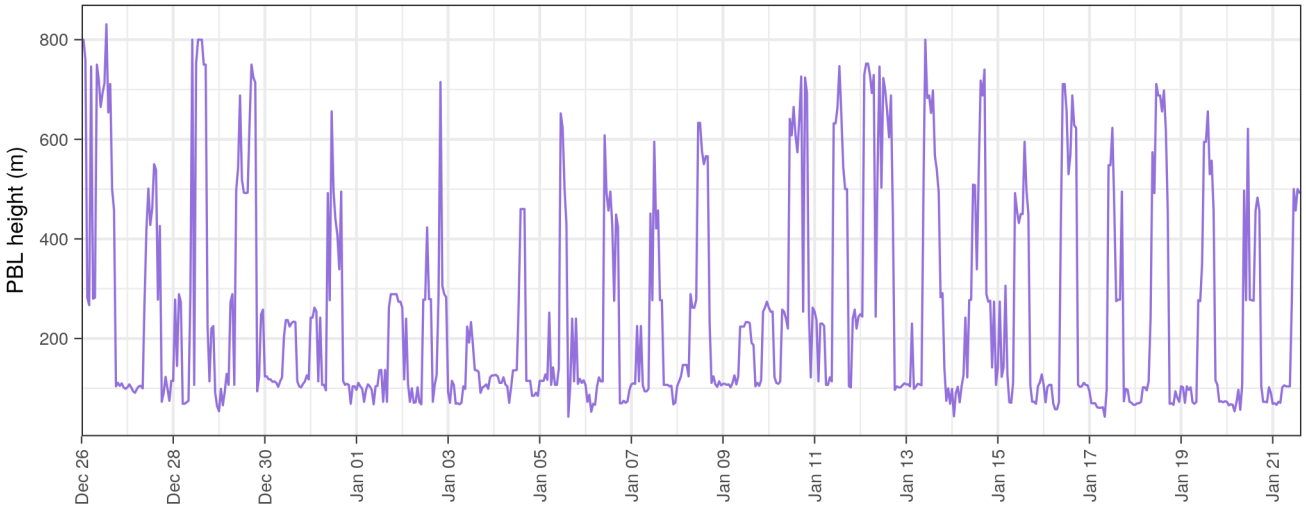

Figure S9. Hourly time series of modelled Planetary Boundary Layer height by GRAL over the urban area of Modena for the second period.

S7 Daily emission modulations

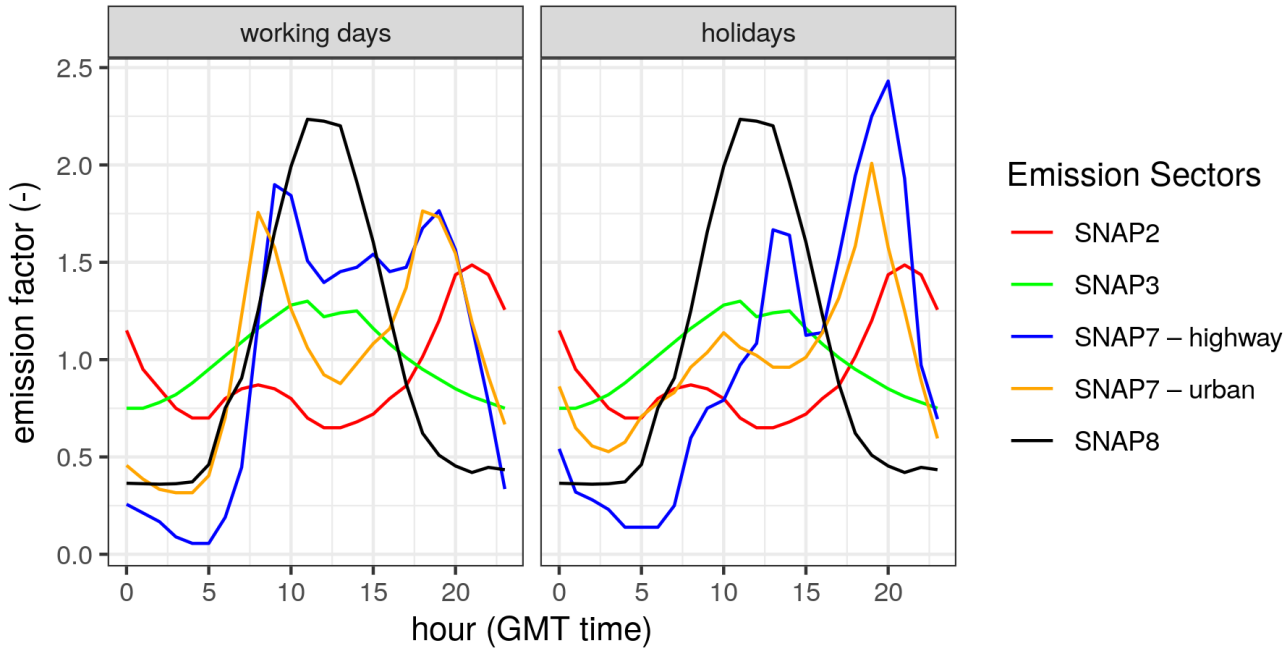

Figure S10. Daily modulation profile of BC emission sources on working days (on the left) and holidays (on the right).

S8 Fleet composition and BC traffic emission factors

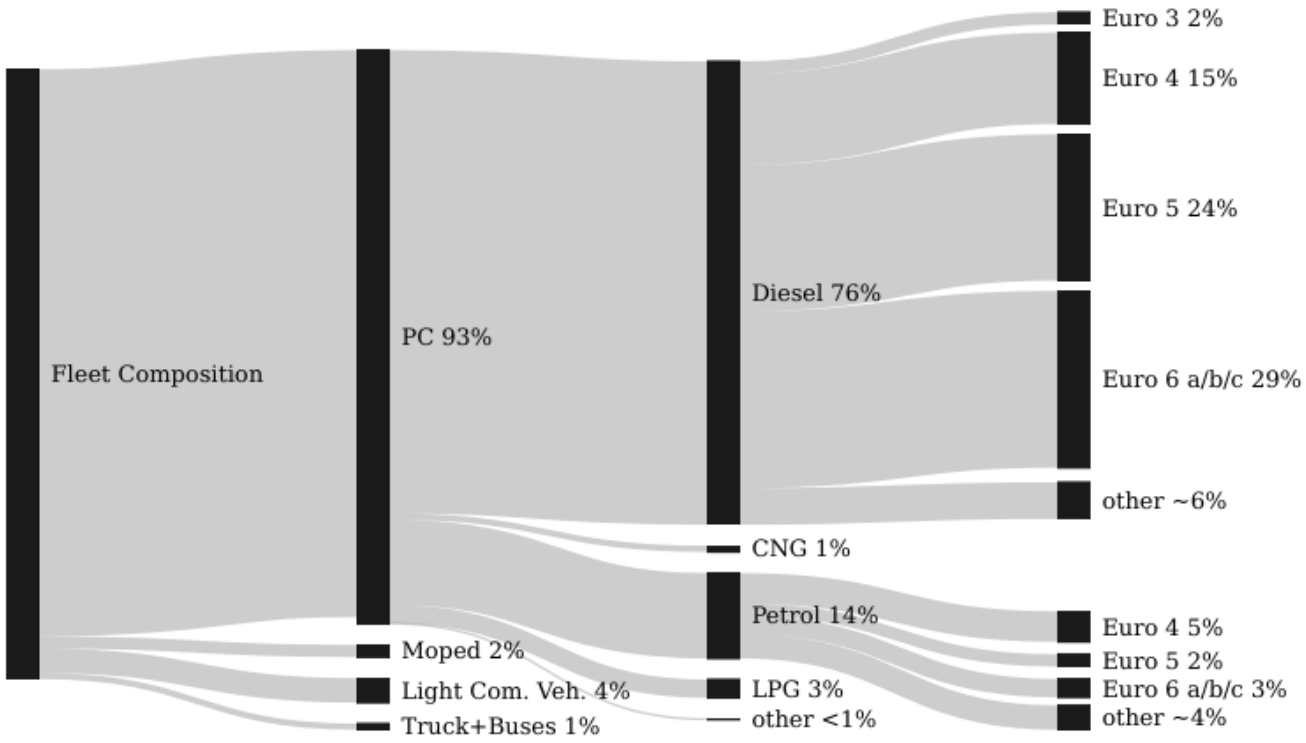

Figure S11. Local Fleet Composition. The number of registered vehicles is normalised taking into account the estimated total kilometres travelled by each vehicle category per year.

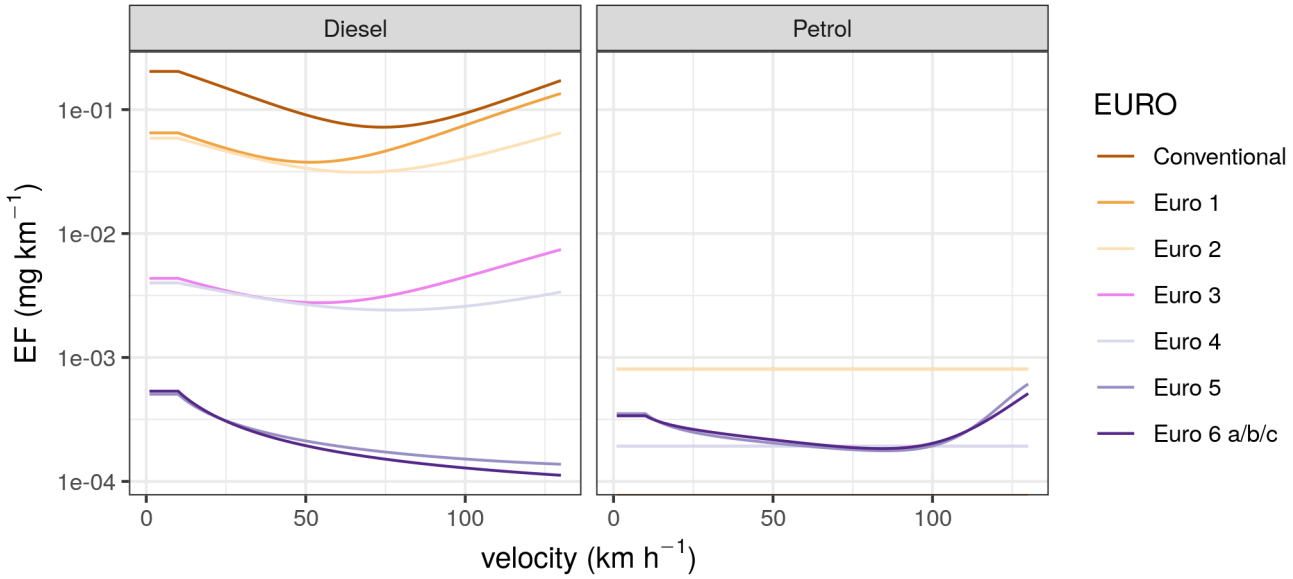

Figure S12. BC emission factors (EF) of diesel and petrol passenger cars as a function of travelling speed, as implemented in the VERT R package used in this study to estimate exhaust vehicle emissions. EF function for Petrol Conventional and Euro 1 overlaps with that of Euro 2. The same is for the curves of Petrol Euro 3 and Euro 4.

References

Bernardoni, V., Pileci, R. E., Caponi, L., and Massabò, D.: The Multi-Wavelength Absorption Analyzer (MWAA) Model as a Tool for Source and Component Apportionment Based on Aerosol Absorption Properties: Application to Samples Collected in Different Environments, Atmosphere, 8, 218, https://doi.org/10.3390/atmos8110218, number: 11 Publisher: Multidisciplinary Digital Publishing Institute, 2017.

Ghermandi, G., Fabbi, S., Bigi, A., Veratti, G., Despini, F., Teggi, S., Barbieri, C., and Torreggiani, L.: Impact assessment of vehicular exhaust emissions by microscale simulation using automatic traffic flow measurements, Atmospheric Pollution Research, 10, 1473–1481, https://doi.org/10.1016/j.apr.2019.04.004, 2019.

Massabò, D., Caponi, L., Bernardoni, V., Bove, M. C., Brotto, P., Calzolai, G., Cassola, F., Chiari, M., Fedi, M. E., Fermo, P., Giannoni, M., Lucarelli, F., Nava, S., Piazzalunga, A., Valli, G., Vecchi, R., and Prati, P.: Multi-wavelength optical determination of black and brown carbon in atmospheric aerosols, Atmospheric Environment, 108, 1–12, https://doi.org/10.1016/j.atmosenv.2015.02.058, 2015.

Sandradewi, J., Prévôt, A. S. H., Szidat, S., Perron, N., Alfarra, M. R., Lanz, V. A., Weingartner, E., and Baltensperger, U.: Using Aerosol Light Absorption Measurements for the Quantitative Determination of Wood Burning and Traffic Emission Contributions to Particulate Matter, Environmental Science & Technology, 42, 3316–3323, https://doi.org/10.1021/es702253m, publisher: American Chemical Society, 2008.

Tobler, A. K., Skiba, A., Canonaco, F., Močnik, G., Rai, P., Chen, G., Bartyzel, J., Zimnoch, M., Styszko, K., Nęcki, J., Furger, M., Różański, K., Baltensperger, U., Slowik, J. G., and Prevot, A. S. H.: Characterization of non-refractory (NR) PM_1 and source apportionment of organic aerosol in Kraków, Poland, Atmospheric Chemistry and Physics, 21, 14 893–14 906, https://doi.org/10.5194/acp-21-14893-2021, publisher: Copernicus GmbH, 2021.

Zotter, P., Herich, H., Gysel, M., El-Haddad, I., Zhang, Y., Močnik, G., Hüglin, C., Baltensperger, U., Szidat, S., and Prévôt, A. S. H.: Evaluation of the absorption Ångström exponents for traffic and wood burning in the Aethalometer-based source apportionment using radiocarbon measurements of ambient aerosol, Atmospheric Chemistry and Physics, 17, 4229–4249, https://doi.org/10.5194/acp-17-4229-2017, publisher: Copernicus GmbH, 2017.